Ionics (2019) 25:3611–3621
https://doi.org/10.1007/s11581-019-02953-2

ORIGINAL PAPER

The porous spherical Mn and Ti co-doped Li_2FeSiO_4/C cathodes material for lithium-ion batteries

Ping Liu [1,2] · Yong Gong [1,2] · Song Nie [1,2] · Qingshan Fu [1,2] · Lin Li [1,2] · Naiqiang Liu [1,2] · Jian Chen [1,2]

Received: 11 October 2018 / Revised: 20 February 2019 / Accepted: 1 March 2019 / Published online: 23 April 2019

Abstract

$Li_2Fe_{1-x-y}Mn_xTi_ySiO_4$/C ($x = 0.05$~$0.20$, $y = 0.02$~0.08), a porous spherical cathode material for lithium-ion batteries, has been prepared by combining the sol-gel, spray drying, and microwave synthesis method, and co-doped Li_2FeSiO_4 with the Mn^{2+} and Ti^{4+}on the iron site. The effects of Mn^{2+} and Ti^{4+} co-doping on the crystal structure, microstructure, and electrochemical performance Li_2FeSiO_4 were investigated by X-ray diffraction (XRD), scanning electron microscopy (SEM), transmission electron microscopy (TEM), and electrochemical tests. The results showed that the modified sample ($Li_2Fe_{0.81}Mn_{0.15}Ti_{0.04}SiO_4$/C), when x and y are 0.15 and 0.04, respectively, has the higher specific capacity and better cycle stability as well as lower impedance and better reversibility. Its electronic conductivity reached 6.85×10^{-4} S/cm, lithium-ion diffusion coefficient reached 1.65×10^{-13} cm^2/s, and initial charge/discharge–specific capacity reaches 197.7/187.8 mAh/g and high capacity retention of 78% after 20 charge/discharge cycles at 2 C. According to the study, the Li_2FeSiO_4/C cathodes material of Mn and Ti co-substitution at the Fe site could partly make up the disadvantage of single Mn doping, and might provide an effective guide for the dopant incorporation to Li_2FeSiO_4 systems.

Keywords Li_2FeSiO_4 · Bulk phase co-doping · Electrochemical performance · Lithium-ion batteries

Introduction

Silicate polyanion compound materials of lithium electrodes Li_2MSiO_4 (M = Co, Fe, Ni, Mn, etc.) are considered as alternative cathode materials for the next-generation lithium-ion battery (LIB), owing to their competitive advantages such as high theoretical capacity exceeding 330 mAh/g, safety, highly stability, environment friendly, abundant natural resources, and so forth [1–7]. Among several polyanionic compounds, orthorhombic metasilicate crystal ($Pnm2_1$, Pnmb, and $P2_1/n$), Li_2FeSiO_4 has become a hot spot of orthosilicate cathode materials because of some disadvantages of other materials, such as low electrochemical activity for Li_2CoSiO_4 [8, 9] and rapidly decreased capacity for Li_2MnSiO_4 and Li_2NiSiO_4 during charging and discharging [10–12]. However, the actual power density of Li_2FeSiO_4 (LFS) is low due to its low electronic conductivity and poor lithium ion mobility [13–15]. In order to solve these issues, researchers have made a number of efforts to enhance the electrochemical performance of Li-ion batteries such as carbon coating, [16, 17] cationic doping, [4, 6, 7, 18–21] and nano-crystallization [22]. For example, synthesized Li_2FeSiO_4/C/GO with citric acid and GO as carbon sources by Huang [23] et al. exhibited the better electrochemical properties than Li_2FeSiO_4, whose initial discharge capacity was 155 mAh/g and capacity retention achieved 96.8% after 30 cycles at 5 C. Nevertheless, carbon coating only increases the ionic conductivity of Li_2FeSiO_4 particles high on the surface and between particles, but not within Li_2FeSiO_4 particles, which limit its practical application to a certain degree. In addition, Kokal [24] et al. found that the radius of Mn^{2+} is similar to that of Fe^{2+} ion, and appropriate amount of Mn^{2+} substituted for Fe^{2+} can form solid solution in Li_2FeSiO_4 crystal and achieving a higher storage capacity because Mn^{2+}/Mn^{3+} can be oxidized to Mn^{3+}/Mn^{4+} to enable

Electronic supplementary material The online version of this article (https://doi.org/10.1007/s11581-019-02953-2) contains supplementary material, which is available to authorized users.

✉ Jian Chen
jchenzg@aliyun.com

[1] School of Materials Science and Engineering, Sichuan University of Science & Engineering, Zigong 643000, China

[2] Sichuan province Key Laboratory for Corrosion and Protection of Material, Sichuan University of Science & Engineering, Zigong 643000, China

$Li_2Fe_{1-x}Mn_xSiO_4$ to achieve more than one Li^+-ion per formula unit extraction/insertion at a wide potential window. However, this process was usually accompanied with serious capacity fade and drastic poor rate capability due to the structural instability of $Li_2Fe_{1-x}Mn_xSiO_4$ caused by Jahn-Teller effect during the first few cycles and subsequent upon further cycling [25]. Fortunately, Zheng [26] et al. showed that the n-type doping introduced by Ti^{4+} can not only improve the conductivity of Li_2FeSiO_4, but also enhance the coupling between SiO_4 and FeO_4 tetrahedrons through the hybridization of d-orbital electrons, so as to enhance the stability of cathode materials.

In this article, to overcome drastic capacity fade and poor rate capability of Mn-doped Li_2FeSiO_4, we report a porous spherical cathode material, which are $Li_2Fe_{0.81}Mn_{0.15}Ti_{0.04}SiO_4/C$ synthesized by sol-gel, spray drying, and microwave synthesis method for lithium-ion batteries. And flat charge/discharge plateau accompanied by the extraction/insertion of more than one Li^+-ions in a narrow potential window 1.5–4.8 V for $Li_2Fe_{0.81}Mn_{0.15}Ti_{0.04}SiO_4/C$ (polymorph with orthorhombic structure, $P2_1/n$ space group) was obtained [27]. Therefore, the co-doped Li_2FeSiO_4 with the Mn^{2+} and Ti^{4+}on the iron site can not only show an obvious improvement in specific capacity, but also have some positive effect on the rate and cycling performance [28]. In addition, X-ray diffraction (XRD), scanning electron microscopy (SEM), transmission electron microscopy (TEM), atomic force microscope (AFM), and electrochemical tests were used to investigate systematically the effects of Mn^{2+} and Ti^{4+} co-doping on the crystal structure, morphology, and electrochemical performance.

Experimental

Synthesis of $Li_2Fe_{1-x-y}Mn_xTi_ySiO_4/C$ composite

The synthesis of $Li_2Fe_{1-x-y}Mn_xTi_ySiO_4/C$, which is porous spherical, was carried out by a novel method of sol-gel, spray drying, and microwave synthesis. The main product was 0.04 M $Li_2Fe_{1-x-y}Mn_xTi_ySiO_4/C$. It was prepared as follow: Firstly, dispersing carbon source (starch) in de-ionized water to obtain an aqueous solution with a carbon content of 6 wt.% in a beaker, which 6 wt.% was the theoretical carbon content of $Li_2Fe_{1-x-y}Mn_xTi_ySiO_4/C$ (the actual coated carbon content of is 5. 47 wt.%). Secondly, taking iron source ($FeNO_3{\cdot}9H_2O$) and manganese source (Mn $(CH_3COO)_2{\cdot}4H_2O$) (the molar mass of Fe and Mn ratio is 1-*x*:*x*, $x = 0.05, 0.10, 0.15, 0.20$) blended by mechanical stirring, then added 0.08 M lithium source (CH_3COOLi) and 0.2 g of surfactant (PVP) with continually mechanical stirring, followed by adding 0.04 M silicon source (SiO_2-sol) and a specific amount of titanium source (nano-TiO_2) (the molar mass of Fe, Mn, and Ti ratio is 1-*x*-*y*:*x*:y, $y = 0.02, 0.04, 0.06, 0.08$), blended by sonication at room temperature for 20 min. Thirdly, the sol mixture was turned into a sphere morphology, by spray drying with the inlet temperature at 200 C and out let temperature at 100 °C. Then, the precursor was dried in vacuum at 110 °C for 8 h and pressed into piece with tablet press (30 MPa). Finally, the piece was placed in a tube furnace and heated at different heat treatment temperature and time in an argon atmosphere.

Physico-chemical characterization

The X-ray diffraction (XRD, Bruker/D2 PHASER) was used to characterize the phase composition of the materials in reflection mode with Cu-$K_{\alpha 1}$ radiation ($\lambda = 1.5406$ nm), in the 2θ range between 10° and 80° in steps of 0.02° with an integration time of 2 s per step. The morphology and structure were evaluated by a field emission scanning electron microscopy (FESEM, Quanta 450 FEG), a transmission electron microscopy (TEM, FEI Tecnai G2 F30), and an atomic force microscope (AFM, E-sweep). The actual carbon content was evaluated by an elemental analyzer (ELEMENTAR, Vario EL cube).

Electrochemical characterization

Electrochemical characterization was done to test the electrochemical performance of $Li_2Fe_{1-x-y}Mn_xTi_ySiO_4/C$ cathodes material, which was performed by CR2032 cion cell. The cathode electrode was prepared by blending 80 wt.% active material ($Li_2Fe_{1-x-y}Mn_xTi_ySiO_4/C$), 10 wt.% conductive additives (Super-P), and 10 wt.% waterborne adhesive (LB132) with magnetic stirring to form a slurry. Then, we coated slurry on aluminum foil current collector via doctor blade processing, followed drying under vacuum at 110 °C for 12 h. After that, the electrode film was cut into circular disks, and the average loading of active material is 3 mg/cm^2. Afterward, all the cells were assembled in an argon-filled glove box (Super1220/990/750) with lithium metal as the counter electrode and a polypropylene microporous film (Celgaed2400) in the middle as separator. The electrolyte was a solution of 1 M $LiPF_6$, which dispersed in the mixture of DMC:EMC:EC (the ratio of 1:1:1 by volume). The cells were tested between 1.5 and 4.8 V (vs. Li^+/Li) at room temperature by CT2001A Land battery testing system [29]. The cyclic voltammetry (CV) tests were carried out at room temperature by CH1604E electrochemical workstation with a scanning rate of 0.1 mV/s in the potential window of 1.5 V to 4.8 V. Electrochemical impedance spectroscopy (EIS) was measured at room temperature using CH1604E electrochemical workstation in the frequency range from 0.1 Hz to 100 kHz with an AC voltage of 5 mV.

Results and discussion

Effect of Mn^{2+} doping on $Li_2Fe_{1-x}Mn_xSiO_4/C$ performance

XRD patterns of $Li_2Fe_{1-x}Mn_xSiO_4/C$ ($x = 0.00$, 0.05, 0.10, 0.15, 0.20) samples are showed in Fig. 1. It can be seen that $Li_2Fe_{1-x}MnxSiO_4/C$ doped with different Mn^{2+} amounts exhibit no impurity phase (PDF#01-077-4374), diffraction peaks were all relatively sharply, and the crystallinity was high. Above all, different Mn^{2+} doping dosage did not change the crystal structure of Li_2FeSiO_4/C, and $Li_2Fe_{1-x}Mn_xSiO_4/C$ still belonged to $P2_1/n$ structure [30, 31]. Doping the dopant ions to replace the position of original ions will form a solid solution and change the unit cell parameters, and thus cause the shift of diffraction peak. When 2θ is 24.3°, this diffraction peak which matches the (111) crystal face of Li_2FeSiO_4 shows obvious shift to the left when doped Mn^{2+} replaced the position of Fe^{2+} in Li_2FeSiO_4 lattice. With increasing the mixing amount of Mn^{2+}, more the shift could be found from the XRD patterns. Moreover, the lattice parameters were obtain by Cell-Refinement function of the Jade5.0 software during the analysis of the XRD results and are listed in Table 1. From Table 1, with the doped dosage of Mn^{2+}change, the lattice parameters vary significantly. It can be observed a constantly increasement of the unit cell volume with the increased amount of Mn^{2+}. As a result, the diffusion rate and coefficient of lithium ions were boosted by the increase of crystal cell volume, which can expand the diffusion channel of lithium ions and reduce the resistance of lithium ion diffusion.

Table 1 Lattice parameters of $Li_2Fe_{1-x}Mn_xSiO_4/C$ samples

$Li_2Fe_{1-x}Mn_xSiO_4/C$	a/Å	b/Å	c/Å	β/°	V/Å^3
$x = 0$	8.230	5.013	8.236	99.328	335.29
$x = 0.05$	8.237	5.009	8.238	99.346	335.38
$x = 0.10$	8.238	5.014	8.229	99.332	335.40
$x = 0.15$	8.235	5.026	8.231	99.416	336.08
$x = 0.20$	8.241	5.019	8.241	99.324	336.31

The SEM has been adopted to detect the morphology of the $Li_2Fe_{1-x}Mn_xSiO_4/C$ composites, and images of the $Li_2Fe_{1-x}Mn_xSiO_4/C$ composites with the amount of doped Mn^{2+} range from $x = 0.05$ to $x = 0.20$ are shown in Fig. 2. As shown in Fig. 2, all the samples present similar morphology of porous spherical particles and show no obvious agglomeration. The particle size distribution of different samples has also been detected and listed in Table 2. It can be seen from Table 2 that particle size distribution (D_{10}, D_{50}, and D_{90}) and tap density of the as-synthesized $Li_2Fe_{1-x}Mn_xSiO_4/C$ exhibit little wave range with the amount of Mn^{2+} doped vary. The result proved that the amount of Mn^{2+} doping has no effect on the morphology, particle size distribution, and tap density of the synthesized $Li_2Fe_{1-x}Mn_xSiO_4/C$.

Figure 3 shows the typical charge/discharge curves of the cathode with the $Li_2Fe_{1-x}Mn_xSiO_4/C$ ($x = 0.05$, 0.10, 0.15, 0.20) at 1/16 C. It figures that $Li_2Fe_{1-x}Mn_xSiO_4/C$ synthesized by different dosage of doped Mn^{2+} ($x = 0.05$, 0.10, 0.15, and 0.20) reveals the initial charge/discharge capacity of 160.4/145.5 mAh/g, 171.1/152.2 mAh/g, 194.8/171.7 mAh/g, and

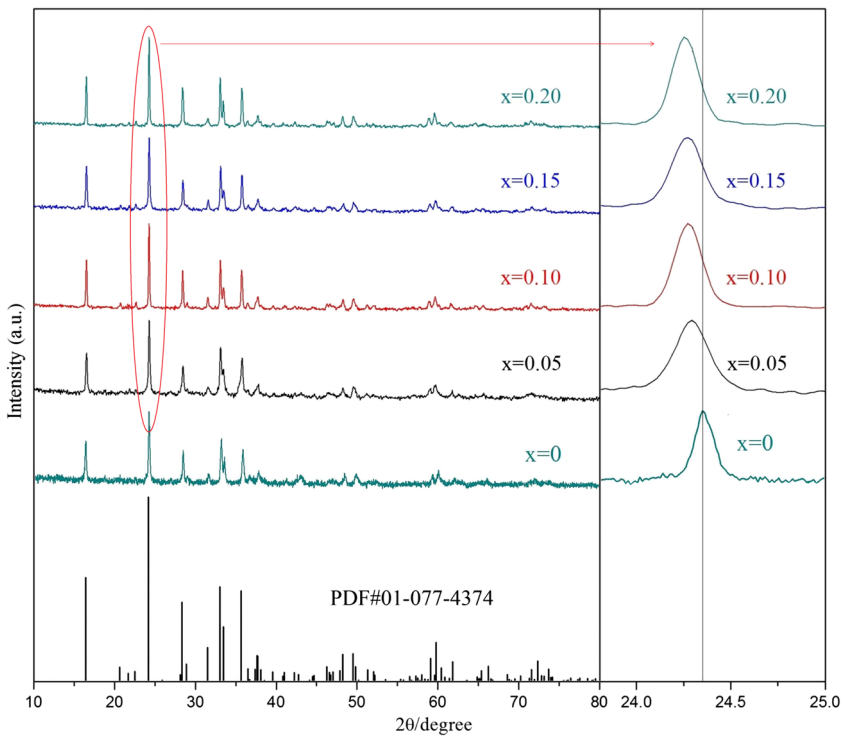

Fig. 1 XRD patterns of $Li_2Fe_{1-x}Mn_xSiO_4/C$ ($x = 0.00$, 0.05, 0.10, 0.15, 0.20)

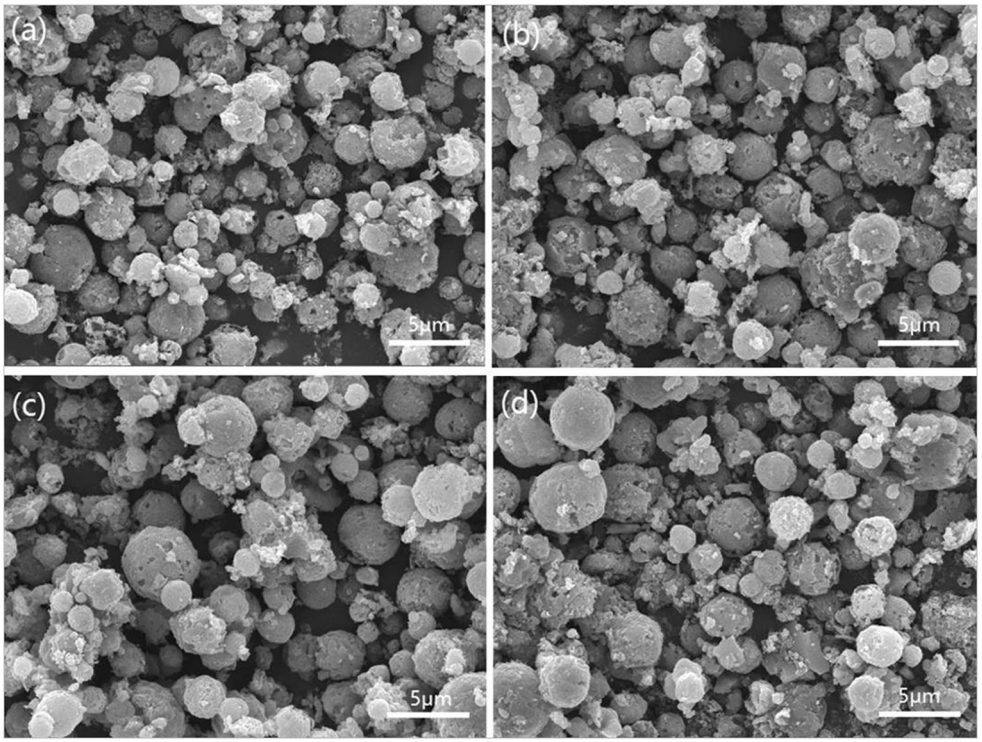

Fig. 2 SEM images of $Li_2Fe_{1-x}Mn_xSiO_4/C$ samples: **a** $x = 0.05$, **b** $x = 0.10$, **c** $x = 0.15$, **d** $x = 0.20$

177.6/128.1 mAh/g, respectively. And the corresponding coulomb efficiency values were 90.7%, 89.0%, 88.1%, and 72.1%, respectively. With the increase of Mn^{2+} content, the charge/discharge capacity of $Li_2Fe_{1-x}Mn_xSiO_4/C$ increased initially and then decreased. When $x > 0.05$ ($x = 0.10$, 0.15, and 0.20), the $Li_2Fe_{1-x}Mn_xSiO_4/C$ reveals higher charge capacity than 166 mAh/g. During the charging process, Mn^{2+} is oxidized to Mn^{4+} and the incorporation of Mn^{2+} into Li_2FeSiO_4/C can incorporate more than one Li^+ [27]. When $x = 0.20$, $Li_2Fe_{1-x}Mn_xSiO_4/C$ owns the lowest specific capacity and coulomb efficiency. After Mn^{2+}/Mn^{3+} is oxidized to Mn^{3+}/Mn^{4+}, it is not reduced to Mn^{2+}/Mn^{3+} and combined with O^{2-} to generate MnO_4 tetrahedron to restore to the original vacancy [30].

In Fig. 4, the curves show the cycling performance of $Li_2Fe_{1-x}Mn_xSiO_4/C$ cathode at 0.1 C. The $Li_2Fe_{1-x}Mn_xSiO_4/C$ synthesized by different Mn^{2+}/Mn^{3+} quantity ($x = 0.05$, 0.10, 0.15, and 0.20) delivers a specific capacity of 131.8 mAh/g, 136.1 mAh/g, 147.8 mAh/g, and 93.8 mAh/g, respectively. And the related capacity retention ratio was 93.7%, 92.6%, 89.8%, and 76.2%, respectively. During the cycling process, $Li_2Fe_{1-x}Mn_xSiO_4/C$ synthesized with different amounts of Mn^{2+}/Mn^{3+} exhibit different degrees of capacity decay, and $Li_2Fe_{0.8}Mn_{0.2}SiO_4/C$ decays the most seriously. Since $Li_2Fe_{0.8}Mn_{0.2}SiO_4/C$ has the highest content of Mn^{2+}/Mn^{3+}, it has a high chemical activity to be oxidized into Mn^{3+}/Mn^{4+}, and it may react with electrolyte but not with O^{2-} to form tetrahedron, which results in the material maintaining a certain structure. Therefore, the Li^+ fails to be re-embedded into $Li_2Fe_{0.8}Mn_{0.2}SiO_4/C$ after extracted. Capacity decreases as the number of circle increases, and the number of Li^+ that can insert into $Li_2Fe_{0.8}Mn_{0.2}SiO_4/C$ has decreased [32].

Table 2 Particle size distribution of $Li_2Fe_{1-x}Mn_xSiO_4/C$ samples

$Li_2Fe_{1-x}Mn_xSiO_4/C$	D_{10}/μm	D_{50}/μm	D_{90}/μm	Tap density/g cm^{-3}
$x = 0.05$	1.73	6.67	39.62	1.19
$x = 0.10$	1.65	6.42	42.59	1.17
$x = 0.15$	2.16	5.98	37.81	1.20
$x = 0.20$	1.54	6.93	35.72	1.22

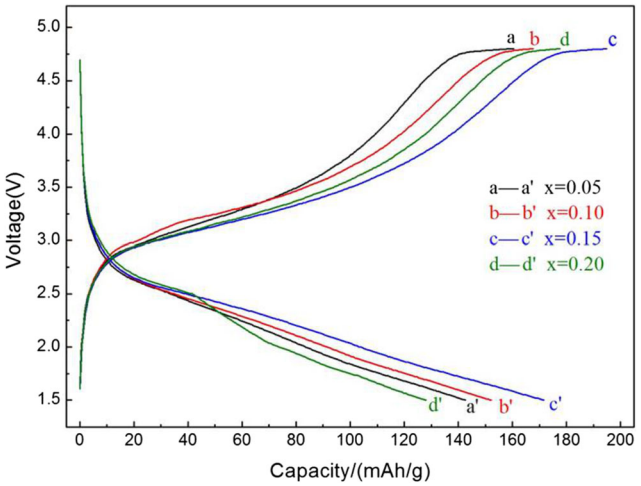

Fig. 3 Charge/discharge curves of $Li_2Fe_{1-x}Mn_xSiO_4/C$ ($x = 0.05$, 0.10, 0.15, 0.20)

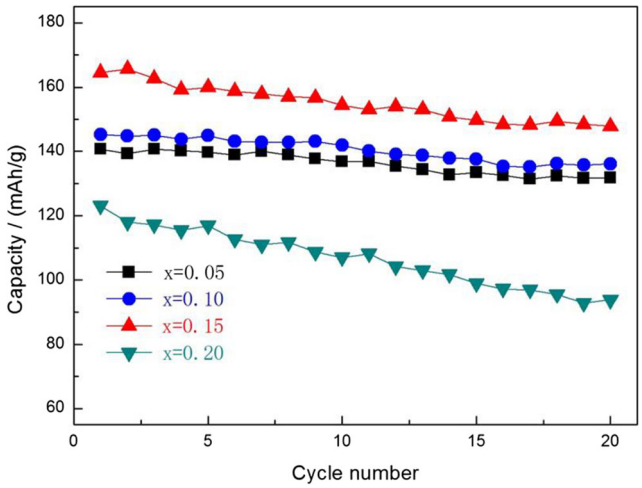

Fig. 4 Cycling performance of $Li_2Fe_{1-x}Mn_xSiO_4/C$ ($x = 0.05, 0.10, 0.15, 0.20$) samples

Effect of Ti^{4+} doping on $Li_2Fe_{0.85-y}Mn_{0.15}Ti_ySiO_4/C$ performance

XRD patterns of $Li_2Fe_{0.85-y}Mn_{0.15}Ti_ySiO_4/C$ ($y = 0.02, 0.04, 0.06, 0.08$) are shown in Fig. 5. According to the XRD result, $Li_2Fe_{0.85-y}Mn_{0.15}Ti_ySiO_4/C$ doped by different Ti^{4+} quantities all belong to $P2_1/n$ structure (PDF#01-077-4374) [29, 30]. Their diffraction peaks are sharp and with high crystallinity. The impurities of Fe, Mn, Ti, and Ti-compounds did not appear in the XRD patterns, indicating that different Ti^{4+} quantities have been doped into the lattice of $Li_2Fe_{0.85-y}Mn_{0.15}Ti_ySiO_4/C$. With the increase of Ti^{4+} doping, the diffraction peak of crystal plane (111) shifted significantly to the left, because the addition of Ti^{4+} to $Li_2Fe_{0.85-y}Mn_{0.15}Ti_ySiO_4/C$ lattice changes the cell parameters. As shown in Table 3, the crystal lattice volume of $Li_2Fe_{0.85-y}Mn_{0.15}Ti_ySiO_4/C$ increased by raising the Ti^{4+} dosage.

Figure 6 shows the SEM diagram of $Li_2Fe_{0.85-y}Mn_{0.15}Ti_ySiO_4/C$ ($y = 0.02, 0.04, 0.06, 0.08$). According to the images, the morphology of $Li_2Fe_{0.85-y}Mn_{0.15}Ti_ySiO_4/C$ shows no change with different amounts of Ti^{4+}. It can be seen from Table 4 that theTi^{4+} doping has no influence on the particle size distribution and tap density of the synthesized $Li_2Fe_{0.85-y}Mn_{0.15}Ti_ySiO_4/C$.

In Fig. 7, the curves show that the $Li_2Fe_{0.85-y}Mn_{0.15}Ti_ySiO_4/C$ ($y = 0.02, 0.04, 0.06, 0.08$) charge/discharge at 1/16 C. It can be seen that the initial charge/discharge capacity of $Li_2Fe_{0.85-y}Mn_{0.15}Ti_ySiO_4/C$ with different Ti^{4+} content ($y = 0.02, 0.04, 0.06$, and 0.08) was 191.3/176.7 mAh/g, 197.7/187.8 mAh/g, 194.7/177.7 mAh/g, and 186.8/155.4 mAh/g, respectively. And the coulomb efficiency was 92.4%, 95.0%, 91.3%, and 83.2%, respectively. With the increase of Ti^{4+} content, the charge-discharge capacity of $Li_2Fe_{0.85-y}Mn_{0.15}Ti_ySiO_4/C$ increased firstly and then decreased. When $y = 0.04$, a discharge specific capacity of $Li_2Fe_{0.81}Mn_{0.15}Ti_{0.04}SiO_4/C$ exhibits 187.8 mAh/g, which is equal to 1.13 Li^+-ion de-intercalate from the crystal lattice. In addition, the coulomb efficiency reaches to 95.0%, suggesting that the incorporation of Ti^{4+} into the tetrahedron may make the Mn^{2+}/Mn^{3+} and the MnO_4 tetrahedron generated by O^{2-} return to the original vacancy [27].

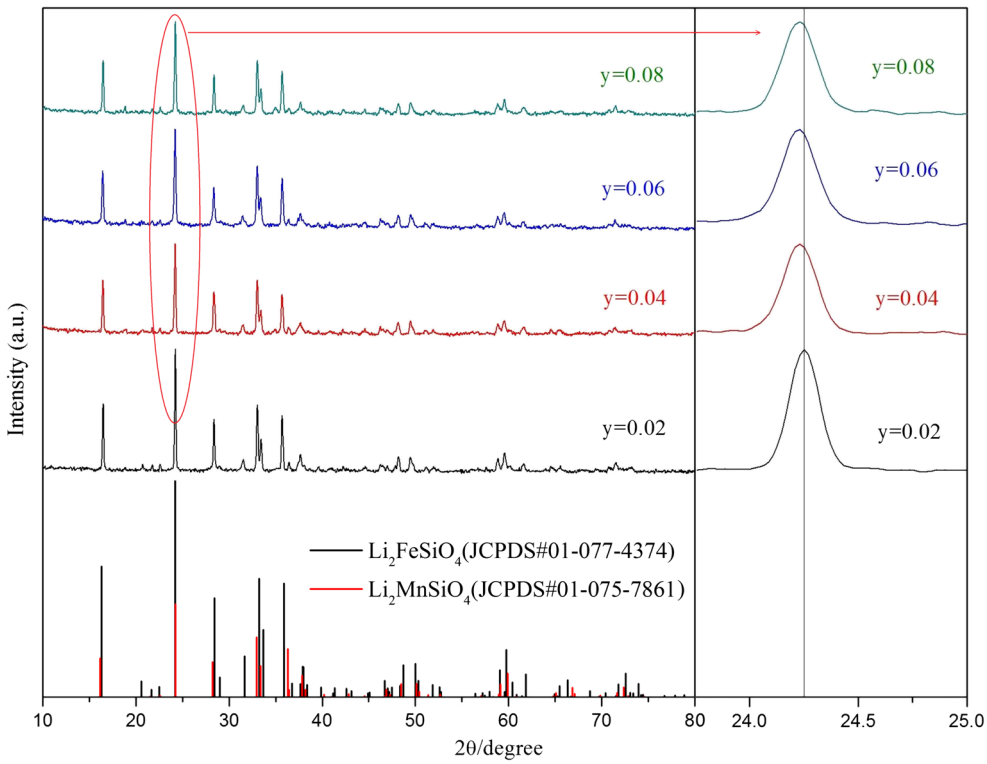

Fig. 5 XRD patterns of $Li_2Fe_{0.85-y}Mn_{0.15}Ti_ySiO_4/C$ ($y = 0.02, 0.04, 0.06, 0.08$)

Table 3 Lattice parameters of $Li_2Fe_{0.85-y}Mn_{0.15}Ti_ySiO_4/C$ samples

$Li_2Fe_{0.85-y}Mn_{0.15}Ti_ySiO_4/C$	a/Å	b/Å	c/Å	β/°	V/Å^3
$y = 0$	8.241	5.019	8.241	99.324	336.31
$y = 0.02$	8.239	5.022	8.242	99.349	336.49
$y = 0.04$	8.246	5.021	8.239	99.347	336.59
$y = 0.06$	8.244	5.017	8.253	99.331	336.83
$y = 0.08$	8.253	5.018	8.245	99.352	336.92

Table 4 Particle size distribution of $Li_2Fe_{0.85-y}Mn_{0.15}Ti_ySiO_4/C$ samples

$Li_2Fe_{1-x}Mn_xSiO_4/C$	D_{10}/μm	D_{50}/μm	D_{90}/μm	Tap density/g cm^{-3}
$y = 0.02$	1.57	6.58	37.13	1.15
$y = 0.04$	1.84	6.27	39.91	1.20
$y = 0.06$	1.61	6.46	42.65	1.18
$y = 0.08$	2.01	6.87	38.74	1.17

In Fig. 8, the curves show the cycle performance of the $Li_2Fe_{0.85-y}Mn_{0.15}Ti_ySiO_4/C$ at 0.1 C. It can be seen that the $Li_2Fe_{0.85-y}Mn_{0.15}Ti_ySiO_4/C$ synthesized by different mixing Mn^{2+} quantity $y = 0.02$, 0.04, 0.06, and 0.08 delivers a specific capacity of 168 mAh/g, 177.3 mAh/g, 159.2 mAh/g, and 138.1 mAh/g, respectively. The capacity retention ratio was 97. 8%, 98.3%, 96.0%, and 92.7%, respectively. The cycling stability of $Li_2Fe_{0.85-y}Mn_{0.15}$ Ti_ySiO_4/C improved firstly and then decreased with the increase of Ti^{4+} dosage. Therefore, the addition of appropriate amount of Ti^{4+} into $Li_2Fe_{0.85-y}Mn_{0.15}$ Ti_ySiO_4/C not only stabilizes the crystal structure, but also enhances cyclic performance of $Li_2Fe_{0.85-y}Mn_{0.15}Ti_ySiO_4/C$. And furthermore, the synergistic doped Ti^{4+} and Mn^{2+} improves the specific capacity of the material.

Characterization of $Li_2Fe_{0.81}Mn_{0.15}Ti_{0.04}SiO_4/C$

The electrochemical performance of $Li_2Fe_{0.81}Mn_{0.15}Ti_{0.04}SiO_4/C$ is the most outstanding, when the Fe, Mn, and Ti mole ratio of $Li_2Fe_{1-x-y}Mn_xTi_ySiO_4/C$ is $1\text{-}x\text{-}y{:}x{:}y = 0.81{:}0.15{:}0.04$. Figure 9 shows the SEM diagram of $Li_2Fe_{0.81}Mn_{0.15}Ti_{0.04}SiO_4/C$. The figure shows that thickness of carbon coating layer on $Li_2Fe_{0.81}Mn_{0.15}Ti_{0.04}SiO_4$ is about 15 nm, indicating Mn^{2+} and Ti^{4+} doped $Li_2Fe_{0.81}Mn_{0.15}Ti_{0.04}SiO_4/C$ after no change of starch of pyrolytic carbon $Li_2Fe_{0.81}Mn_{0.15}Ti_{0.04}SiO_4$ coating effect.

Figure 10 shows the rate and cycling performance of $Li_2Fe_{0.81}Mn_{0.15}Ti_{0.04}SiO_4/C$ cathode. The long-term cycling performance of the $Li_2Fe_{0.81}Mn_{0.15}Ti_{0.04}SiO_4/C$ cathode has been performed at 0.5 C for 50 circles. The specific capacity is 161.8 mAh/g after 50 cycles at 0.5 C times. And the rate performance of the batteries has been tested by a gradual raising current density from 0.2 C to 2 C. A high specific capacity can be observed from the rate performance test. The $Li_2Fe_{0.81}Mn_{0.15}Ti_{0.04}SiO_4/C$ cathode displays specific capacity of 172.4 mAh/g, 162.8 mAh/g, 147.1 mAh/g, and 126.0 mAh/g at 0.2 C, 0.5 C, 1 C, and 2 C, respectively. Moreover, when we lowered the current density to 0.2 C and

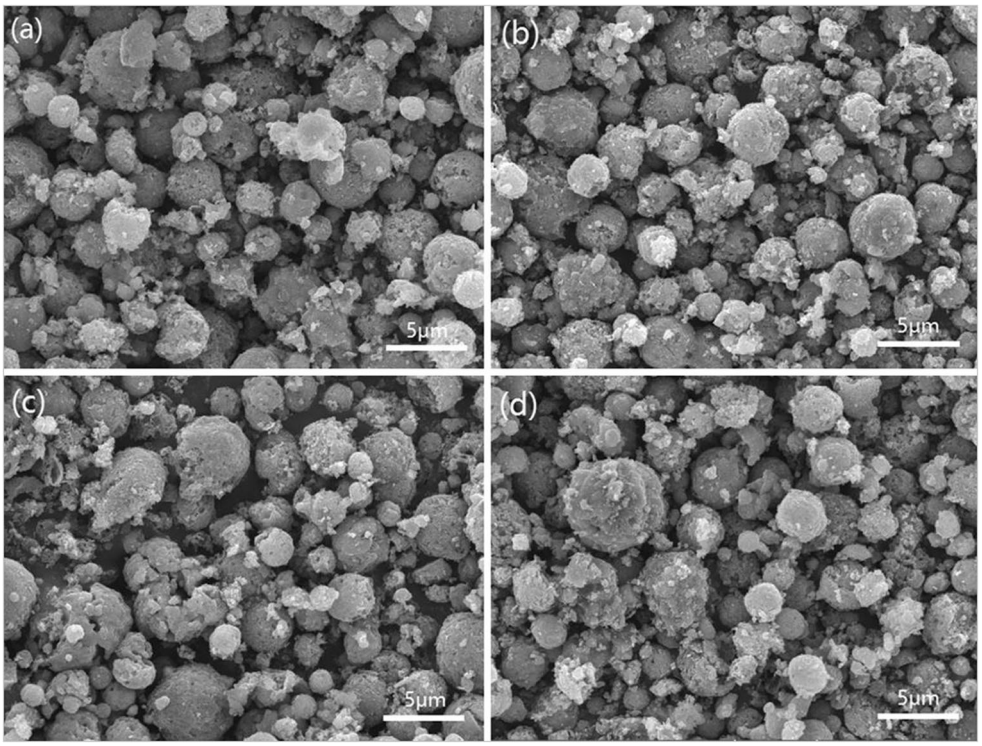

Fig. 6 SEM images of $Li_2Fe_{0.85-y}Mn_{0.15}Ti_ySiO_4/C$ samples: **a** $y = 0.02$, **b** $y = 0.04$, **c** $y = 0.06$, **d** $y = 0.08$

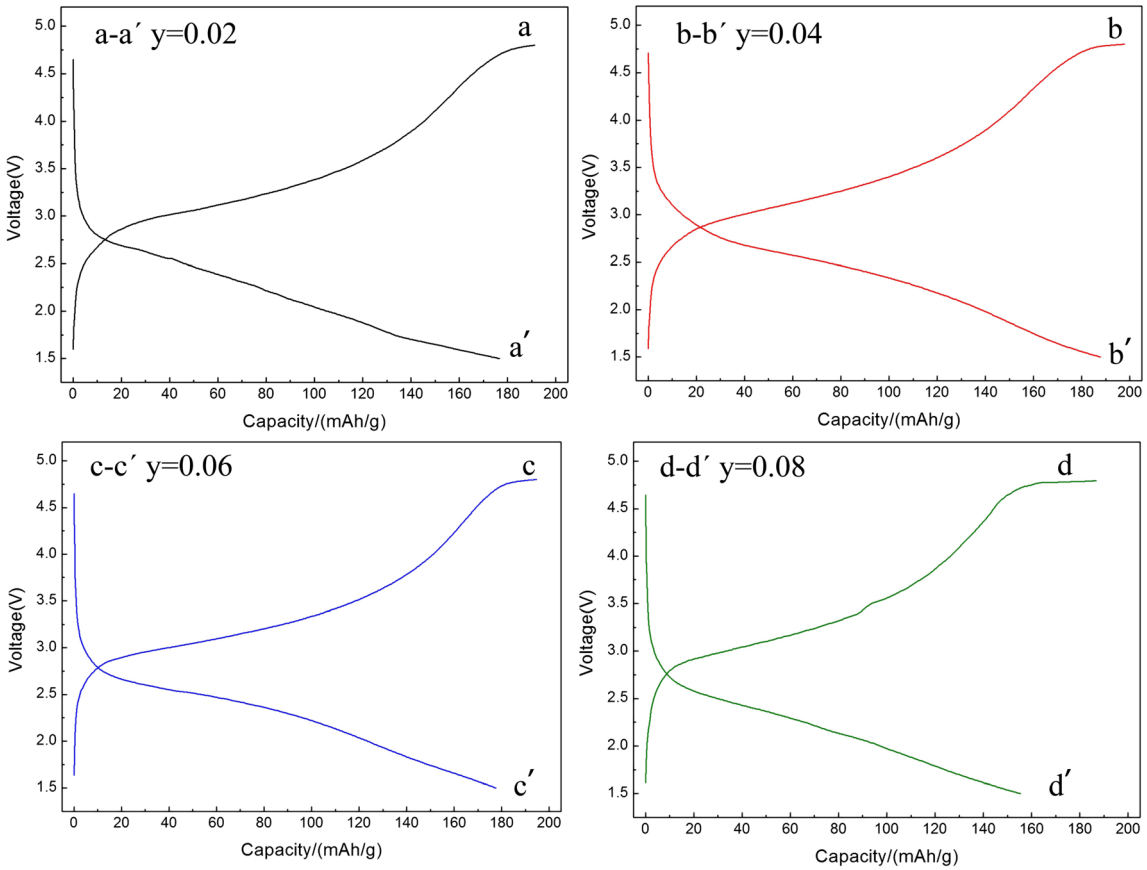

Fig. 7 Charge/discharge curves of $Li_2Fe_{0.85-y}Mn_{0.15}Ti_ySiO_4/C$ sample: **a** $y = 0.02$, **b** $y = 0.04$, **c** $y = 0.06$, **d** $y = 0.08$

cycled for 10 times, the $Li_2Fe_{0.81}Mn_{0.15}Ti_{0.04}SiO_4/C$ cathode still shows a specific capacity of 172.5 mAh/g. Even when the current density went back to 0.5 C, the specific capacity could return to 161.8 mAh/g. This outstanding rate performance indicates the high electrical conductivity and the fast Li^+-ion conductivity of the $Li_2Fe_{0.81}Mn_{0.15}Ti_{0.04}SiO_4/C$ composite. The electrical conductivity characterization of

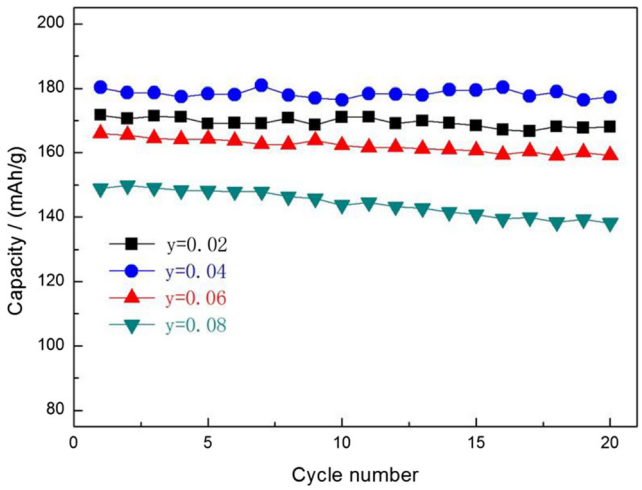

Fig. 8 Cycling performance of $Li_2Fe_{0.85-y}Mn_{0.15}Ti_ySiO_4/C$ ($y = 0.02$, 0.04, 0.06, 0.08)

$Li_2Fe_{0.81}Mn_{0.15}Ti_{0.04}SiO_4/C$ exhibits a result of 6.85×10^{-4} S/cm, thus three times higher than the Li_2FeSiO_4 coated by starch carbon. And the long-term cycling performance of the $Li_2Fe_{0.81}Mn_{0.15}Ti_{0.04}SiO_4/C$ cathode has been performed at 0.5 C for 50 circles. The specific capacity is 161.8 mAh/g after 50 cycles at 0.5 C times. The improved long-term cycling performance indicates that co-doped appropriate Mn^{2+} and Ti^{4+} into $Li_2Fe_{1-x-y}Mn_xTi_ySiO_4/C$ could keep the crystal structure of the material from collapsing. Although pure Mn^{2+}doped can enhance the specific capacity, the cycling performance of the batteries will be worse. Overall, the Mn^{2+} and Ti^{4+}co-doped, which is a novel method, demonstrates a feasible way to achieve a stable structure and good cyclic performance of this kind Li_2FeSiO_4 material.

Figure 11 is CV curves for the Li_2FeSiO_4/C and $Li_2Fe_{0.81}Mn_{0.15}Ti_{0.04}SiO_4/C$ cathode at initial three circles. The scanning rate was 0.1 mV/s in the potential window of 1.5–4.8 V. During the negative scanning process, the reduction peaks exhibits lithium implantation behavior concentrated at about 2.4 V, with good repeatability. During the scanning circle from second and third, the peak shifts to the left and increases the area. This is the structural rearrangement to a more stable structure after the first cycle, which means the amount of lithium embedded increases. In the forward scanning process, the oxidation peak Li_2FeSiO_4/C, which is

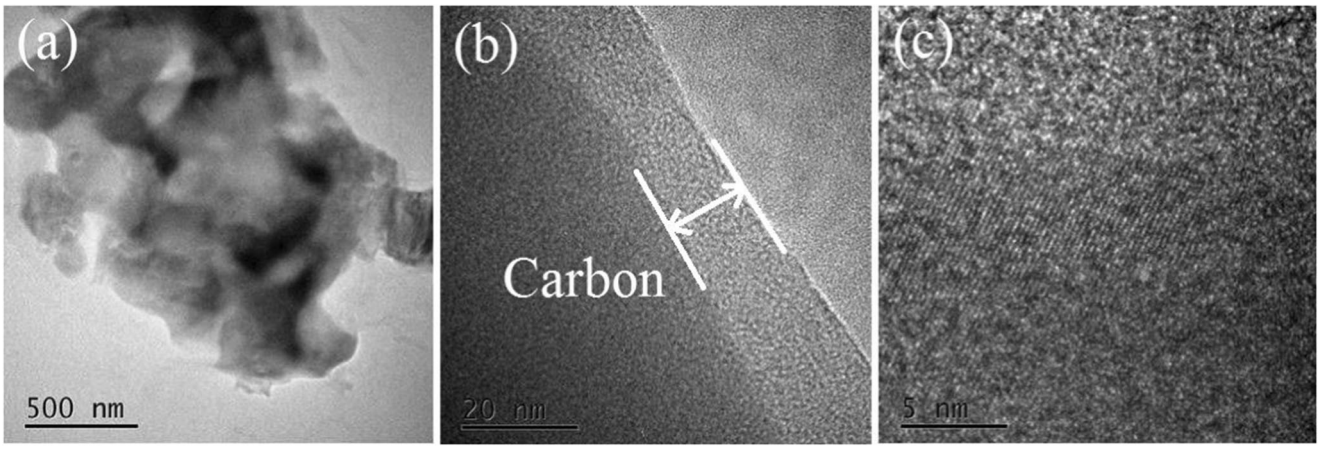

Fig. 9 Morphology characterization of $Li_2Fe_{0.81}Mn_{0.15}Ti_{0.04}SiO_4/C$ sample. **a** TEM images of $Li_2Fe_{0.81}Mn_{0.15}Ti_{0.04}SiO_4/C$ sample, **b** carbon-coated layer, and **c** HRTEM images

manifested as lithium removal behavior, has a "transition" weak peak at 3.6 V in addition to the main peak type of 3.3 V, which can be attributed to the oxidation of Fe^{2+} to Fe^{3+} [15, 33–35]. The $Li_2Fe_{0.81}Mn_{0.15}Ti_{0.04}SiO_4/C$ obtained an overlapped oxidation peak curve at about 3.3 V, thus implying the stable structure during cycling. $Li_2Fe_{0.81}Mn_{0.15}Ti_{0.04}SiO_4/C$ with high potential of oxidation peak is a slowly weakening trend, suggesting that Mn^{2+} and Ti^{4+} doped are conducive to oxidation reaction of Fe^{3+}/Fe^{4+}, Mn^{3+}/Mn^{4+}, and Ti^{3+}/Ti^{4+} [14, 36–39]. Thus, we speculated that the Mn^{2+}- and Ti^{4+}-doped $Li_2Fe_{0.81}Mn_{0.15}Ti_{0.04}SiO_4/C$ have increased structural stability during de/intercalation.

As shown in Fig. 12, the electrochemical impedance spectra (EIS) have been conducted to illustrate the electrochemical performance of Li_2FeSiO_4/C and $Li_2Fe_{0.81}Mn_{0.15}Ti_{0.04}SiO_4/C$ cathode after cycled 50 times at 0.5 C. The charge transfer resistance Rct in the high-frequency areas of Li_2FeSiO_4/C and $Li_2Fe_{0.81}Mn_{0.15}Ti_{0.04}SiO_4/C$ cathode is 130 and 35 Ω, respectively. The slope of $Li_2Fe_{0.81}Mn_{0.15}Ti_{0.04}SiO_4/C$ low-frequency area is significantly greater than that of Li_2FeSiO_4/C. This indicated that Mn^{2+} and Ti^{4+} co-doped increased the conductivity and significantly reduced the electrochemical impedance caused by the charge transfer on the surface of the electrode. According to formula (1) and (2), Li^+ diffusion rate of the Li_2FeSiO_4/C and $Li_2Fe_{0.81}Mn_{0.15}Ti_{0.04}SiO_4/C$ cathode could be calculated, [40, 41] where D is the diffusion coefficient of lithium ion, R is the gas constant (8.314 J/K mol^{-1}), T is the room temperature in our experiment (298 K), A is the surface area of the electrode (1.13 cm^2), n is the number of the electrons per molecule attending the electronic transfer reaction which is 1, F is the Faraday constant (96,500 C/mol), C is the concentration of lithium ion in electrolyte (0.039 mol/cm^3 for Li_2FeSiO_4) [38]. R_D is the ohmic resistance, R_L is the charge

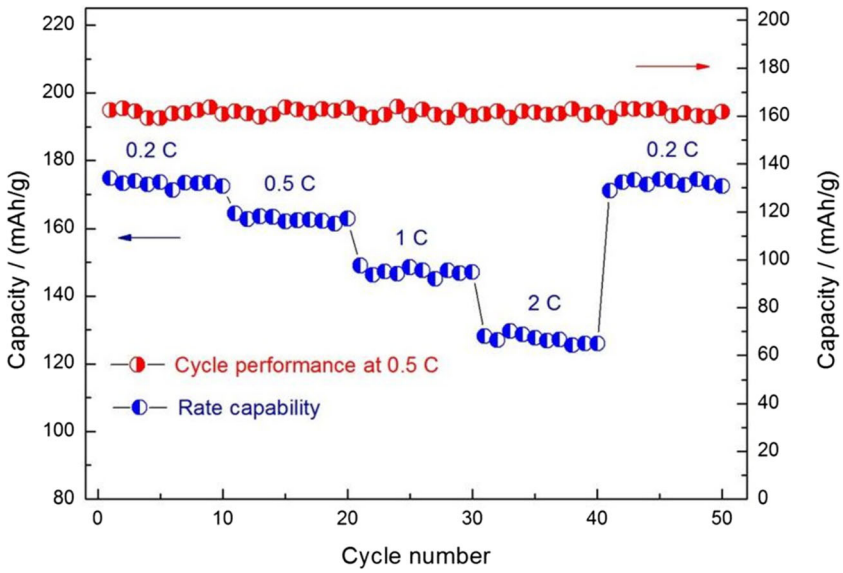

Fig. 10 Rate and cycling performance of $Li_2Fe_{0.81}Mn_{0.15}Ti_{0.04}SiO_4/C$ cathode

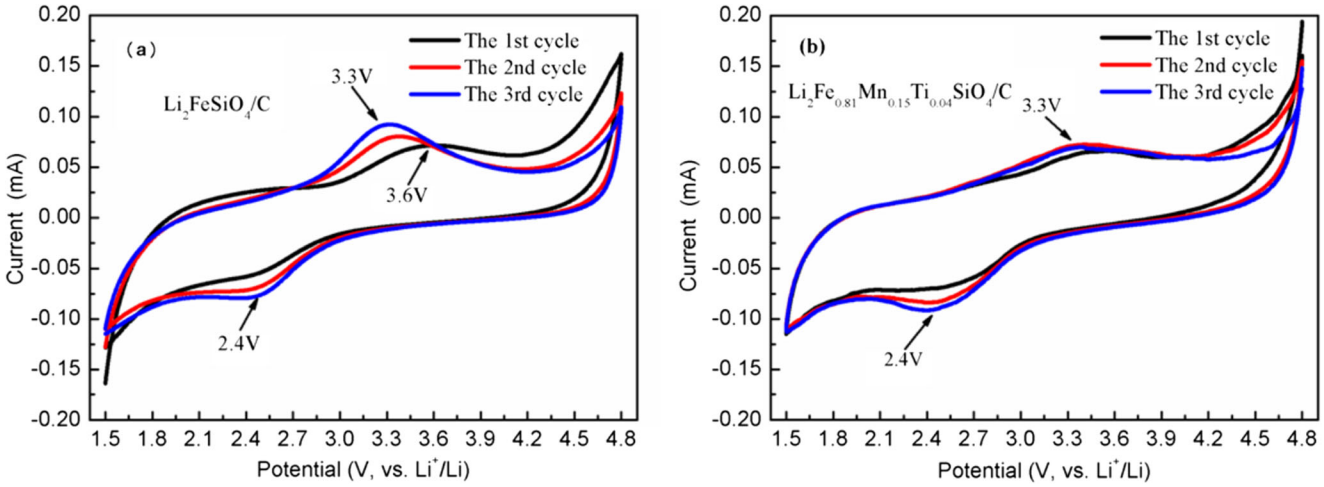

Fig. 11 The CV profiles of **a** Li_2FeSiO_4/C and **b** $Li_2Fe_{0.81}Mn_{0.15}Ti_{0.04}SiO_4/C$ cathode

transfer resistance, ω is the angular frequency in the low-frequency region, and σ is the Warburg factor, which can be obtained from the slopes of linear fitting of Z'' versus $\omega^{-1/2}$ plots in Fig. 12.

$$D = \frac{R^2T^2}{2A^2n^4F^4C^2\sigma^2} \quad (1)$$

$$Z_{re} = R_D + R_L + \sigma\omega^{-1/2} \quad (2)$$

The obtained σ value of Li_2FeSiO_4/C and $Li_2Fe_{0.80}Mn_{0.15}Ti_{0.05}SiO_4/C$ is 31.5 Ω $s^{-1/2}$ and 29.7 Ω $s^{-1/2}$, respectively. Finally, the $Li_2Fe_{0.80}Mn_{0.15}Ti_{0.05}SiO_4/C$ has fast Li^+ diffusion rate of 1.65×10^{-13} cm^2/s and Li_2FeSiO_4/C of 1.47×10^{-13} cm^2/s, which is consistent with the outstanding rate performance of $Li_2Fe_{0.80}Mn_{0.15}Ti_{0.05}SiO_4/C$. As confirmed by the diffusion coefficient, the $Li_2Fe_{0.80}Mn_{0.15}Ti_{0.05}SiO_4/C$ cathode showed higher lithium ion conductivity. It could be attributed to that the co-doped Mn^{2+} and Ti^{4+} increase the cell volume and extending the Li^+ diffusion path in and out of $Li_2Fe_{0.81}Mn_{0.15}Ti_{0.04}SiO_4/C$ particles [6, 26, 42].

To study the effect of structural stability of Li_2FeSiO_4/C and $Li_2Fe_{0.81}Mn_{0.15}Ti_{0.04}SiO_4/C$ composite electrode during cycling, SEM and AFM were used to observe the surface morphology of the electrode before and after cycling (Fig.S1 and S2). It can be seen that the electrode surface becomes smooth after charge/discharge testing, and the morphology has no obvious change. The Li_2FeSiO_4/C and $Li_2Fe_{0.81}Mn_{0.15}Ti_{0.04}SiO_4/C$ can still maintain spherical structure after cycling [43].

We also have compared our results with some recent reported heteroatom-doped Li_2FeSiO_4/C materials as shown in Table S1. The result demonstrates that the $Li_2Fe_{0.81}Mn_{0.15}Ti_{0.04}SiO_4/C$ with porous spherical structure prepared by combining the sol-gel, spray drying, and microwave synthesis method shows a higher initial discharge specific capacity and faster lithium ion diffusion rate.

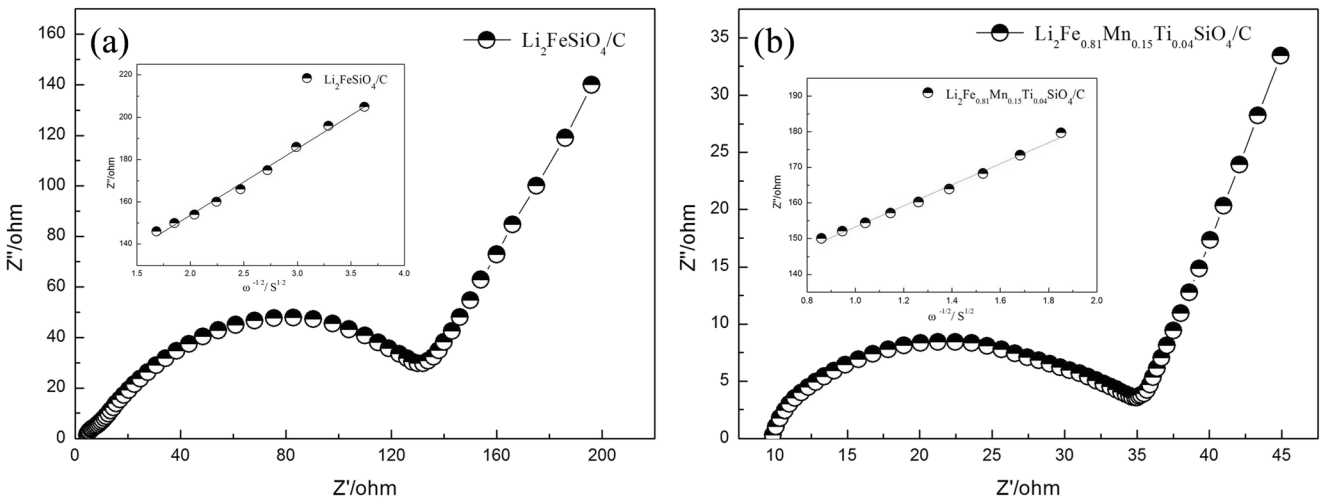

Fig. 12 Electrochemical impedance spectra of **a** Li_2FeSiO_4/C and **b** $Li_2Fe_{0.81}Mn_{0.15}Ti_{0.04}SiO_4/C$ cathode

Conclusions

Porous spherical $Li_2Fe_{1-x-y}Mn_xTi_ySiO_4/C$ ($x = 0.05$~0.20, $y = 0.02$~0.08) composite has been successfully prepared via a novel method of sol-gel, spray drying, and microwave synthesis for cathode material. This method carried out the bulk phase modified by co-doping Mn^{2+} and Ti^{4+} on the iron site and a thick layer carbon coating at the same time. Co-doping Ti^{4+} into $Li_2Fe_{0.85}Mn_{0.15}SiO_4/C$ can make Mn^{2+} and O^{2-} form tetrahedron again and return to the original vacancy to avoid the collapse of the crystal structure, and thus improves the stability of the material. In addition, Ti^{4+} can work with Mn^{2+} to increase the specific capacity of $Li_2Fe_{0.85-y}Mn_{0.15}Ti_ySiO_4/C$. When mole ratio of Fe and Ti in $Li_2Fe_{0.85-y}Mn_{0.15}Ti_ySiO_4/C$ is $0.85-y:y$ ($y = 0.04$), $Li_2Fe_{0.81}Mn_{0.15}Ti_{0.04}SiO_4/C$ has a higher specific capacity and better cycle stability. The initial discharge specific capacity was 187.8 mAh/g, which is equal to 1.13 Li^+ from $Li_2Fe_{0.81}Mn_{0.15}Ti_{0.04}SiO_4/C$ embedded in lattice. After cycling for 10 times at 0.2 C, the specific capacity was 172.5 mAh/g, and 161.8 mAh/g after cycled for 50 times at 0.5 C. In addition, by co-doping Mn^{2+} and Ti^{4+}, the electric conductivity of $Li_2Fe_{0.81}Mn_{0.15}Ti_{0.04}SiO_4/C$ increased to 6.85×10^{-4} S/cm. Most importantly, co-doped appropriate Mn^{2+} and Ti^{4+} into $Li_2Fe_{1-x-y}Mn_xTi_ySiO_4/C$ could keep the stability of crystal structure from collapsing, and point out a feasible way to achieve a stable structure and good cyclic performance of Li_2FeSiO_4 material.

Funding The work was financially supported by the National Nature Science Foundation of China (grant no. 51572177), the Foundation of Sichuan Science and Technology department project (grant no. 2017JY0158), the Foundation of Sichuan science and technology project (grant no. 2017GZ0121), and the Foundation of Graduate Innovation Fund of Sichuan University of Science and Engineering (grant no. y2018048).

References

1. Dominko R, Bele M, Kokalj A, Gaberscek M, Jamnik J (2007) Li_2MnSiO_4 as a potential Li-battery cathode material[J]. J Power Sources 174(2):457–461
2. Dompablo AD, Armand M, Tarascon JM et al (2006) On-demand design of polyoxianionic cathode materials based on electronegativity correlations: an exploration of the $LiMSiO_4$ system (M=Fe, Mn, o, Ni)[J]. Electrochem Commun 8(8):1292–1298
3. Qu L, Luo D, Fang S, Liu Y, Yang L, Hirano SI, Yang CC (2016) Mg-doped Li_2FeSiO_4/C as high-performance cathode material for lithium-ion battery[J]. J Power Sources 307:69–76
4. Li L, Han E, Yang P, et al (2018) Study on electrochemical performance of Mg-doped Li_2FeSiO_4 cathode material for Li-ion batteries[J]. Ionics 1–10
5. Dominko R, Bele M, Gaberscek M et al (2006) Structure and electrochemical performance of Li_2MnSiO_4 and Li_2FeSiO_4 as potential Li-battery cathode materials[J]. Electrochem Commun 8(2):217–222
6. Li T, Jiang X, Gao K et al (2016) Electrochemical investigations of Mn and Al co-doped Li_2FeSiO_4/C cathodes for Li-ion battery[J]. J Chin Chem Soc 63(9):800–807
7. Sivaraj P, Abhilash KP, Nalini B et al (2018) Structure, dielectric, and temperature-dependent conductivity studies of the Li_2FeSiO_4/C nano cathode material for lithium-ion batteries[J]. Ionics:1–16. https://doi.org/10.1007/s11581-018-2685-1
8. Wu S, Zhang J, Zhu Z et al (2007) Structural and electronic properties of the Li-ion battery cathode material Li_xCoSiO_4[J]. Curr Appl Phys 7(6):611–616
9. Zhang C, Chen Z, Zeng Y, Zhang Z, Li J (2014) Insights into changes of lattice and electronic structure associated with electrochemistry of Li_2CoSiO_4 polymorphs[J]. J Phys Chem C 118(14):7351–7356
10. Politaev VV, Petrenko AA, Nalbandyan VB, Medvedev BS, Shvetsova ES (2007) Crystal structure, relations and electrochemical properties of monoclinic Li_2MnSiO_4[J]. J Solid State Chem 180(3):1045–1050
11. Panda MR (2014) Investigations on structural and electrical propertise of Li_2NiSiO_4 [J]. Int J ChemTech Res 6(6):1962–1964
12. Guo HJ, Li LM, Li XH et al (2009) Effects of roasting temperature and modification on properties of Li_2FeSiO_4/C cathode [J]. J Power Sources 189(1):45–50
13. Bai J, Gong Z, Lv D, Li Y, Zou H, Yang Y (2012) Nanostructured $0.8Li_2FeSiO_4/0.4Li_2SiO_3/C$ composite cathode material with enhanced electrochemical performance for lithium-ion batteries[J]. J Mater Chem 22(24):12128–12132
14. Yang J, Kang X, He D, Peng T, Hu L, Mu S (2013) Hierarchical shuttle-like Li_2FeSiO_4, as a highly efficient cathode material for lithium-ion batteries[J]. J Power Sources 242(35):171–178
15. Nytén A, Abouimrane A, Armand M, Gustafsson T, Thomas JO (2005) Electrochemical performance of Li_2FeSiO_4 as a new Li-battery cathode material[J]. Electrochem Commun 7(2):156–160
16. Zhao Y, Wu C, Li J, Guan L (2013) Long cycling life of Li_2MnSiO_4 lithium battery cathodes under the double protection from carbon coating and graphene network[J]. J Mater Chem A 1(12):3856–3859
17. Shin HC, Chung KY, Cho BW, et al (2009) Improved electrochemical properties of the Li_2MSiO_4 (M=Mn, Fe) by carbon coating and doping[C]//Meeting Abstracts. The Electrochemical Society, Pennington, vol 3, pp 168
18. Zhang S, Deng C, Fu BL, Yang SY, Ma L (2010) Effects of Cr doping on the electrochemical properties of Li_2FeSiO_4 cathode materials for lithium-ion batteries [J]. Electrochim Acta 55(28):8482–8489
19. Zhang S, Deng C, Fu BL et al (2009) Doping effects of magnesium on the electrochemical performance of Li_2FeSiO_4 for lithium ion batteries [J]. J Electroanal Chem 644:150–154
20. Lv X, Zhao X, Wu S et al (2018) Fe–Si networks and charge/discharge-induced phase transitions in Li_2FeSiO_4 cathode materials[J]. Phys Chem Chem Phys 20(21):14557–14563
21. Zhang Y, Huo QY, Du PP et al (2012) Advances in new cathode material $LiFePO_4$, for lithium-ion batteries[J]. Synth Met 162(13–14):1315–1326
22. Lv DP, Wen W, Huang XK et al (2011) A novel Li_2FeSiO_4/C composite: synthesis, characterization and high storage capacity [J]. J Mater Chem 21:9506–9512
23. Huang XB, You YY, Ren YR et al (2015) Spray drying-assisted synthesis of hollow spherical Li_2FeSiO_4/C particles with high performance for Li-ion batteries[J]. Solid State Ionics 278:203–208
24. Kokalj A, Dominko R, Mali G, Meden A, Gaberscek M, Jamnik J (2007) Beyond one-electron reaction in Li cathode materials: designing $Li_2Mn_xFe_{1-x}SiO_4$[J]. Chem Mater 19(15):3633–3640
25. Li YX, Gong ZL, Yang Y (2007) Synthesis and characterization of Li_2MnSiO_4/C nanocomposite cathode material for lithium ion batteries[J]. J Power Sources 174(2):528–532

26. Yang J, Zheng J, Kang X, Teng G, Hu L, Tan R, Wang K, Song X, Xu M, Mu S, Pan F (2016) Tuning structural stability and lithium-storage properties by d-orbital hybridization substitution in full tetrahedron Li2FeSiO4 nanocrystal[J]. Nano Energy 20:117–125
27. Devaraj S, Kuezma M, Ng CT, Balaya P (2013) Sol-gel derived nanostructured Li2MnSiO4/C cathode with high storage capacity[J]. Electrochim Acta 102(21):290–298
28. Arof AK (2008) Characteristics of $LiMnO_2$ (M=Co, Ni, $Ni_{0.2}Co_{0.8}$, $Ni_{0.8}Co_{0.2}$) powders prepared from solution of their acetates[J]. J Alloys Compd 449(1–2):288–291
29. Yang J, Kang X, Lin HU et al (2013) Synthesis and electrochemical performance of Li_2FeSiO_4/C/carbon nanosphere composite cathode materials for lithium ion batteries[J]. J Alloys Compd 572(572): 158–162
30. Zhong G, Li Y, Yan P, Liu Z, Xie M, Lin H (2010) Structural, electronic, and electrochemical properties of cathode materials Li2MSiO4 (M = Mn, Fe, and Co): density functional calculations[J]. J Phys Chem C 114(8):3693–3700
31. Nishimura S, Hayase S, Kanno R et al (2012) Structure of Li_2FeSiO_4[J]. J Am Chem Soc 130(40):13212–13213
32. Aravindan V, Karthikeyan K, Lee JW, Madhavi S, Lee YS (2011) Synthesis and improved electrochemical properties of Li_2MnSiO_4 cathodes [J]. J Phys D Appl Phys 44(15):152001–152004
33. Wu XZ, Jiang X, Huo QS, Zhang YX (2012) Facile synthesis of Li_2FeSiO_4/C composites with triblock copolymer P123 and their application as cathode materials for lithium ion batteries[J]. Electrochim Acta 80:50–55
34. Singh S, Mitra S (2014) Improved electrochemical activity of nanostructured Li_2FeSiO_4/MWCNTs composite cathode[J]. Electrochim Acta 123:378–386
35. Lv DP, Bai JY, Zhang P, Wu SQ, Li YX, Wen W, Jiang Z, Mi JX, Zhu ZZ, Yang Y (2013) Understanding the high capacity of Li_2FeSiO_4: in situ XRD/XANES study combined with first-principles calculations [J]. Chem Mater 25(10):2014–2020
36. Wang F, Wang YM, Sun DM, Wang L, Yang J, Jia HP (2014) High performance Li_2MnSiO_4 prepared in molten KCl-NaCl for rechargeable lithium ion batteries[J]. Electrochim Acta 119:131–137
37. Liu SK, Xu J, Li DZ, Hu Y, Liu X, Xie K (2013) High capacity Li_2MnSiO_4/C nanocomposite prepared by sol-gel method for lithium-ion batteries[J]. J Power Sources 232:258–263
38. Qiu H, Yue H, Wang X, Zhang T, Zhang M, Fang Z, Zhao X, Chen G, Wei Y, Wang C, Zhang D (2017) Titanium-doped Li_2FeSiO_4/C composite as the cathode material for lithium-ion batteries with excellent rate capability and long cycle life[J]. J Alloys Compd 725:860–868
39. Deng C, Zhang S, Yang SY, Fu BL, Ma L (2011) Synthesis and characterization of $Li_2Fe_{0.97}M_{0.03}SiO_4$ (M = Zn^{2+}, Cu^{2+}, Ni^{2+}) cathode materials for lithium ion batteries[J]. J Power Sources 196(1):386–392
40. Shenouda AY, Liu HK (2008) Electrochemical behaviour of tin borophosphate negative electrodes for energy storage systems[J]. J Power Sources 185(2):1386–1391
41. Shenouda AY, Liu HK (2009) Studies on electrochemical behaviour of zinc-doped LiFePO4 for lithium battery positive electrode[J]. J Alloys Compd 477(1–2):498–503
42. Huang XB, Li X, Wang HY et al (2010) Synthesis and electrochemical performance of Li_2FeSiO_4/C as cathode material for lithium batteries [J]. Solid State Ionics 181(31–32):1451–1455
43. Yi L, Wang X, Wang G, Bai Y, Liu M, Wang X, Yu R (2016) Improved electrochemical performance of spherical Li_2FeSiO_4/C cathode materials via Mn doping for Lithium-ion batteries[J]. Electrochim Acta 222:1354–1364